# Interaction between impurities and solitons in quasi one-dimensional spin-Peierls systems

D. Augier[a], P. Hansen[b], D. Poilblanc[a], J. Riera[a,b], and E. Sørensen[a]

[a] Laboratoire de Physique Quantique & Unité Mixte de Recherche CNRS 5626
Université Paul Sabatier, 31062 Toulouse, France

[b] Instituto de Física Rosario, Consejo Nacional de Investigaciones Científicas y Técnicas y Departamento de Física
Universidad Nacional de Rosario, Avenida Pellegrini 250, 2000-Rosario, Argentina

(February 7, 2008)

The role of the spin-phonon coupling in spin-Peierls chains doped with spin-0 or spin-1 impurities is investigated by various numerical methods such as exact diagonalization, quantum Monte Carlo simulations and Density Matrix Renormalization Group. Various treatments of the lattice, in a fully quantum mechanical way, classically in the adiabatic approximation or using a fixed three-dimensional dimerization pattern are compared. For an isolated chain, strong bonds form between the two spin-$\frac{1}{2}$ sites next to the impurity site, leading to the appearance of magneto-elastic solitons. We also show that these excitations do not bind to spin-0 impurities but are weakly attracted by spin-1 impurities. However, the interchain elastic coupling generates an effective confining potential at the non-magnetic impurity site which can lead to the formation of soliton-impurity bound states. We also predict that a soliton and an antisoliton bound to two impurities on the same chain can annihilate each other when the separation between the impurities is smaller than a critical value depending on the interchain elastic constant.

PACS: 75.10 Jm, 75.40.Mg, 75.50.Ee, 75.30.Hx

## I. INTRODUCTION

Quasi one-dimensional (1D) quantum antiferromagnets can exhibit surprising magnetic properties at low temperature. The recent discovery of the spin-Peierls (SP) transition in the inorganic compounds $CuGeO_3$ (Ref. 1) and $NaV_2O_5$ (Ref. 2) has drawn both experimental and theoretical interest. The chemistry of these compounds indeed allows for the synthesis of large single crystals and consequently the achievement of new experimental studies[3] which were not accessible to the previously known organic SP materials. Nevertheless, these two compounds have quite different behaviors presumably due to the fact that while $NaV_2O_5$ is believed to have quarter-filled ladders, $CuGeO_3$ is well described by weakly coupled spin-$\frac{1}{2}$ Heisenberg chains. In this sense, the present studies are more related to this latter compound.

At a critical temperature, $T_c$, the SP compounds undergo a phase transition driven by the spin-phonon coupling. This SP transition, which is characterized by the opening of a spin gap and a lattice dimerization, is experimentally signaled by an isotropic drop of the magnetic susceptibility revealing the non-magnetic nature of the ground state (GS). A general physical picture can be drawn from the consideration of the exact GS of the frustrated Heisenberg chain at the so-called Majumdar-Ghosh point. The spontaneously dimerized non-magnetic GS is two-fold degenerate, corresponding to two possible dimerization patterns A and B, which are a succession of disconnected singlet dimers. The elementary excitation called soliton (antisoliton) consists of an unpaired spin separating A and B (B and A) patterns[4].

Solitons and antisolitons propagate, then acquiring a dispersion.

For temperatures above the critical temperature $T_c$, quasi-1D SP compounds are usually described as independent uniform AF Heisenberg chains, in some cases including terms describing the frustration present in the system. The nearest neighbor $J$ and next-nearest neighbor $\alpha J$ exchange integrals can then be estimated by a fit of the magnetic susceptibility[5,6]. The high temperature behavior is governed by $J$ and the position of the maximum by the frustration ratio $\alpha$. Values such as $J \approx 160\,K$ and $\alpha \approx 0.36$ have been proposed for $CuGeO_3$ (Ref. 5).

$CuGeO_3$ can be easily doped by substituting magnetic $Ni^{2+}$ or non-magnetic $Zn^{2+}$ impurities to spin-$\frac{1}{2}$ $Cu^{2+}$. A rapid suppression of the spin gap due to impurity doping has been measured by magnetic susceptibility[7] and inelastic neutron scattering[8] experiments. Competition between the antiferromagnetic (AF) and SP phases has also been observed[7,9−13]. Theoretical work analyzing the effects due to the doping by vacancies has been carried out[14−16], assuming a static dimerization.

The coupling to the lattice plays a major role in SP compounds. A description of these systems in terms of a static dimerized Heisenberg chain is widely found in the literature. This approach has some drawbacks: the dimerization is introduced *de facto* in the model and is totally frozen, the lattice cannot adjust to spin fluctuations, which are essential to understand the behavior under high magnetic fields, or to inhomogeneities introduced by impurities.

In this paper, SP spin-lattice models with spin-0 or spin-1 impurities have been studied at $T = 0$ or very low temperature using various numerical techniques such

as Exact Diagonalization (ED)[17], Quantum Monte-Carlo (QMC) and Density Matrix Renormalization Group (DMRG). Emphasis has been put on the appearance of magneto-elastic excitations and their interplay with impurities. A strictly 1D dynamical spin-lattice model is first studied in Sec. II. Non-uniform dynamical or adiabatic lattice distortions are considered and the existence of bound states due to impurities is investigated. The role of the three-dimensional character of the phonons is then considered, first in the simplest description in terms of a static dimerized Heisenberg chain. Bound states between a soliton and a non-magnetic impurity are quantitatively studied in Sec. III. A simple physical picture is also given to explain the spectrum of bound states. In Sec. IV a more involved model is introduced by considering explicitly the elastic coupling between the 1D spin-phonon chains. This model enables us to understand the physical origin of the soliton-impurity bound states.

## II. 1D SPIN-PHONON CHAIN

### A. Models

The key ingredient of the physics of spin-Peierls compounds is the dynamical spin-phonon coupling. A spin-$\frac{1}{2}$ excitation is expected to locally distort the lattice, creating an elastic soliton. Our starting point is the frustrated Heisenberg chain with the parameters $J$ and $\alpha$ defined below. In addition, we assume a linear dependence of the nearest neighbor exchange integral on the relative atomic displacement. Dispersionless phonons of frequency $\Omega$ are considered for sake of simplicity. One then obtains[18−21],

$$\mathcal{H}_{\parallel}^{(d)} = J \sum_i (1 + g(b_i + b_i^\dagger))(\vec{S}_i \cdot \vec{S}_{i+1} - \frac{1}{4})$$
$$+ \alpha J \sum_j \vec{S}_j \cdot \vec{S}_{j+2} + \Omega \sum_i b_i^\dagger b_i, \quad (1)$$

where $b_i^\dagger$ $(b_i)$ is the phononic creation (destruction) operator at site $i$ and $g$ is the magneto-elastic coupling. Note that we have assumed that the magneto-elastic coupling associated with the next-nearest neighbor bonds can be neglected.

The adiabatic limit of Hamiltonian (1) is of great interest. When the phonon frequency $\Omega$ is sufficiently small compared to the spin fluctuation energy scale $J$, the phonon degrees of freedom can be treated classically. The Hamiltonian is then written as,

$$\mathcal{H}_{\parallel}^{(a)} = J \sum_i (1 + \delta_i) \vec{S}_i \cdot \vec{S}_{i+1} + \alpha J \sum_j \vec{S}_j \cdot \vec{S}_{j+2}$$
$$+ \frac{1}{2} K \sum_i \delta_i^2, \quad (2)$$

where $\delta_i$ is the distortion at site $i$, $K$ the string constant $(= \Omega/(2g^2))$ and the last term corresponds to the elastic energy loss. $\delta_i$ is expressed in units so that the magneto-elastic coupling, which can be absorbed in the definition of $K$, is set to unity. It is interesting to notice that the frustration $\alpha$ alone (i.e. $g = 0$) can lead to a dimerized state for $\alpha > \alpha_c \simeq 0.241167$ (Ref. 22,23,6,24,32). In fact, the relevance of $\alpha$ is two fold; (i) it is required to explain qualitatively the properties of the real compounds ($\alpha \simeq 0.36$ has been proposed in $CuGeO_3$) and (ii) it can be used in numerical simulations to reduce the spin-spin correlation length (for $\alpha = 0.5$ and $g = 0$, it is only one lattice unit) and hence to reduce finite size effects.

The substitution of a spin-$\frac{1}{2}$ by a spin-S (S=0 or 1) impurity is then studied using these Hamiltonians on chains with periodic boundary conditions. The impurity is coupled to its first and second nearest neighbors (see Fig. 1). For sake of simplicity, the couplings between two spins-$\frac{1}{2}$ or between a spin-S impurity and one of its spin-$\frac{1}{2}$ neighbors are taken identical, i.e. the same values of $J$, $\alpha$, $g$ and $\Omega$ are considered all along the chain independently of the nature of the spins. For instance, in the case of a spin-1 impurity, the Hamiltonian impurity part is explicitly

$$\mathcal{H}_{imp}^{(d)} = J \sum_l (1 + g(b_l + b_l^\dagger))(\vec{S}_l \cdot \vec{s} - \frac{1}{2})$$
$$+ \alpha J \sum_m \vec{S}_m \cdot \vec{s} + \Omega \sum_l b_l^\dagger b_l \quad (3)$$

where the impurity spin operator is $\vec{s}$ and $l$ $(m)$ refers to its two nearest (next-nearest) neighbors. However, for a spin-0 impurity, the situation is simpler: all links between the impurity and its spin-$\frac{1}{2}$ neighbors are taken as zero. In this case, when $\alpha = 0$, the system corresponds to a chain with open boundary conditions (OBC).
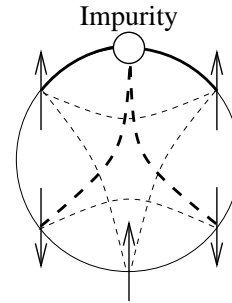
Impurity



FIG. 1. Example of a periodic chain with L=5 spin-$\frac{1}{2}$ sites and an additional impurity. Nearest neighbor (solid lines) and next nearest neighbor (dashed lines) links are plotted. Bold links correspond to the links between the impurity and its spin-$\frac{1}{2}$ neighbors.

### B. Dynamical model

*Numerical technique*: A reliable numerical treatment of

2

Hamiltonian (1) is a difficult task. Indeed, the phononic Hilbert space is infinite, even for a finite chain. Possible approaches such as QMC simulations[26], single-mode approximation[27], or ED with a fixed maximum number of phonons[28] have been proposed. The results obtained in this paper are based on an ED calculation using the coherent states introduced by Fehrenbacher[29]. Preliminary results have been reported in Ref. 19 in the case of pure systems and Ref. 21 for rings with impurities in the absence of frustration. On each site, a two state basis including the phononic vacuum $|0\rangle_i$ and a coherent state $|1\rangle_i$ is considered. The phononic part of the Hamiltonian (1) can be rewritten as $\mathcal{H}_{\mathrm{ph}} = J\lambda \sum_i (b_i + b_i^\dagger)A_i + \Omega \sum_i b_i^\dagger b_i$, where $\lambda$ is a constant and $A_i$ an operator of eigenvalues 0 and 1 (the constant terms subtracted to $\vec{S}_i \cdot \vec{S}_j$ in (1) and (3) have been introduced with this purpose). It is convenient to introduce the coherent state

$$|1\rangle_i = \exp\left(-\eta^2/2\right)\exp\left(\eta\, b_i^\dagger\right)|0\rangle_i,$$

where $\eta$ is a variational parameter. In fact, $|1\rangle_i$ is an eigenstate of the phononic Hamiltonian for fixed $A_i = 1$ provided that $\eta = \eta_0 = -\lambda J/\Omega$. It is shown in Fig. 2(a) that $\eta_0$ is the best value of $\eta$ at small coupling. Furthermore it is a reasonable choice for arbitrary coupling. Therefore we shall assume $\eta = \eta_0$ in the remainder of the paper. Note that the method could be improved by choosing explicitly the optimum $\eta$ that minimizes the energy for each set of parameters. The comparison between this coherent state approach (using $\eta_0$) and a truncation of the phononic Hilbert space retaining two or eight phonon states at each site is illustrated in Fig. 2(b) for the GS energy and the mean phonon number per site. The results are much more accurate using coherent states than when only keeping two phonon states even though
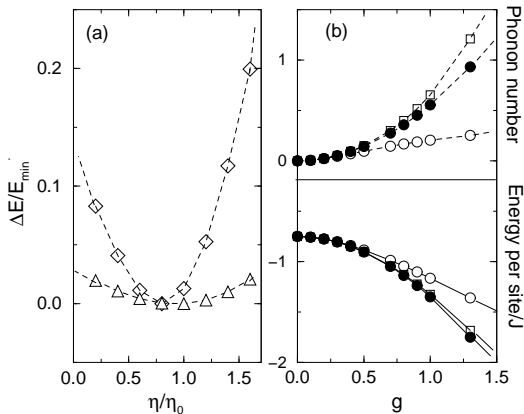


FIG. 2. (a) Relative GS energy of a 4-site chain as a function of the variational parameter $\eta$ for $\alpha = 0.5$, $g = 0.5$, $\Omega = J$ ($\triangle$) and $\alpha = 0$, $g = 1.$, $\Omega = J$ ($\diamond$). (b) GS energy (full line) and mean phonon number (dashed line) per site for a 4-site chain using a two ($\circ$), eight ($\bullet$) phonon states truncation, and using the coherent state approximation with $\eta = \eta_0$ ($\square$) as a function of the magneto-elastic coupling $g$ for $\alpha = 0$ and $\Omega = J$.

both Hilbert spaces have the same sizes. Note that although the GS energy is accurately obtained, the coherent state basis seems to slightly overestimate the mean phonon number. However, even at large couplings, the phonon dynamics is qualitatively preserved. Consequently our non-perturbative approach takes properly into account the effects of the phonons and the results can be checked by comparing to a full phonon calculation on small clusters (typically with $L = 4$ sites) as in Fig. 2(b). This variational treatment of the dynamical phonons hence enables us to handle clusters with up to $L = 16$ sites. Special care is needed for the treatment of the bonds connected to the spin-1 impurity. Indeed, special variational parameters (still corresponding to $\eta_0$) have to be chosen for these bonds because the corresponding $A_i$ operators for the phononic part of the Hamiltonian differ from those of the rest of the chain.

*Results*: Let us summarize the main properties of this model. It has been shown that the GS of this model undergoes at $T = 0$ a spontaneous symmetry breaking toward a dimerized gapped phase in a large region of parameter space[19]. The elementary excitations are characterized as topological solitons, *i.e.* unpaired spins separating the two different dimer patterns. Furthermore solitons $(s)$ and antisolitons $(\bar{s})$ do not bind. More explicitly, one can define the $s\bar{s}$ binding energy as the $p \to \infty$ extrapolation of

$$E_B^{s\bar{s}}(L = 2p) = [E_0(2p, 1) - E_0(2p, 0)] - 2e_s, \qquad (4)$$

where $E_0(l, S_z)$ is the GS energy of a $l$-site periodic chain in the $S^z$ sector. If $l$ is even and $S^z = 0$, $E_0(l, S^z)$ corresponds in fact to the "vacuum" energy, the energy of the pure chain without any topological defect. $e_s$ is the soliton (antisoliton) minimum energy, defined as $e_s = \lim_{p \to \infty}[E_0(2p+1, \frac{1}{2}) - E_0^*(2p+1)]$, where $E_0^*(2p+1)$ is the interpolation between $E_0(2p, 0)$ and $E_0(2p+2, 0)$. Thus, $e_s$ results as the energy difference between an odd chain containing a soliton and an (hypothetical) odd chain without soliton. Similarly, $E_B(s\bar{s}, L)$ is the energy difference between a chain with a $s\bar{s}$ pair and two isolated solitons. Previous studies provide strong evidences that the $s\bar{s}$ binding energy vanishes[19], *i.e.* $E_B = 0$ in the thermodynamic limit in the absence of any explicit dimerization. Similar forms of binding energy will be discussed in the context of impurity-soliton binding.

We first consider the case of a non-magnetic impurity. Typical patterns are shown in Fig. 3(a) for parameters corresponding to CuGeO$_3$. For even chains, the distortion pattern $\delta_i = g\langle b_i^\dagger + b_i \rangle$ rapidly oscillates with a two site period. The equilibrium pattern corresponds to strong bonds (*i.e.* $\delta_i$ positive) next to the impurity. The amplitude $|\delta_i|$ varies along the chain with increasing magnitude for decreasing distance to the impurity. In other words, the impurity being located on site 0, the strongest bonds are the ones connecting sites 1 and 2 and sites L-1 and L. In addition, the average magnitude of the modulation increases with a stronger magneto-elastic coupling or

weaker phonon frequency. The z-component of the spin $\langle S_i^z \rangle$ is zero because the chain is in a dimerized singlet state. For odd chains (Fig. 3(b)), the presence of a soliton at the center of the chain is signaled by a point where $\delta_i$ vanishes and $\langle S_i^z \rangle$ is maximum. This corresponds to the characteristic schematic picture of the soliton as an unpaired spin separating two dimer patterns. Similarly to the even chain case, strong bonds also form at the chain edges. The finite frustration that we have considered here does not seem to change the main features of the pattern (see Ref. 21 for comparison). The fact that the soliton forms at the center of the chain suggests that, contrary to the conclusions of Ref. 30, solitons do not bind to non-magnetic impurities in pure 1D spin-lattice models.
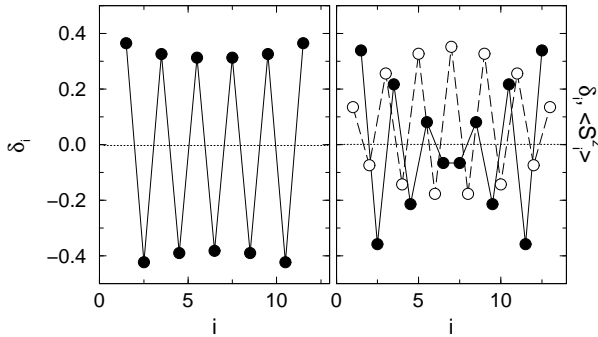


FIG. 3. Distortion $\delta_i$ ($\bullet$) and z-component of the spin $\langle S_i^z \rangle$ ($\circ$) as a function of the site i on (a) a 12-site and (b) a 13-site chain for $\alpha = 0.36$, $g = 0.8$ and $\Omega = J$ with OBC using ED.

In order to be more quantitative, we define a soliton-impurity binding energy similarly to (4),

$$E_B^{I-s}(L = 2p+1) = [E_0'(2p+1, \tfrac{1}{2}) - E_0^*(2p+1)]$$
$$- e_s - e_I, \qquad (5)$$

where $E_0'(l, S^z)$ is the GS energy in the $S^z$ sector of a chain with $l$ spin-$\frac{1}{2}$ sites and with an extra impurity. $e_I$ is an impurity minimum energy, $e_I = \lim_{p\to\infty}[E_0'(2p, 0) - E_0(2p, 0)]$, which indeed corresponds to the energy difference between a chain with and without an impurity.

The results shown in Fig. 4 (a) reveal no binding for any finite chain. Note that finite size effects are small for parameters in the vicinity of the MG point because of the small magnetic correlation length present in this case.

The same calculations can be performed in the case of a spin-1 impurity. The different scaling behaviors in Fig. 4 ($\frac{1}{L^2}$ for the spin-0 and $\frac{1}{L}$ for the spin-1 impurity) suggest that the physics involved is also different. Although a $\frac{1}{L^2}$ behavior may also occur for larger rings with a spin-1 impurity, our data are nevertheless compatible with a small binding between the spin-1 impurity and the soliton.
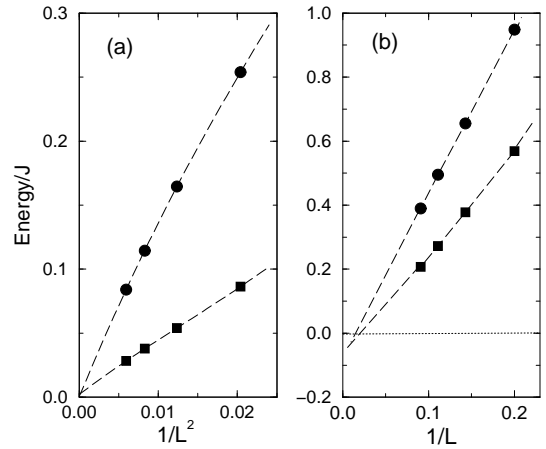


FIG. 4. Soliton-impurity binding energy using ED for $\alpha = 0.5$, $g = 0.4$, $\Omega = 0.3J$ ($\blacksquare$) and $\alpha = 0$, $g = 0.45$, $\Omega = 0.3J$ ($\bullet$) (a) as a function of the inverse square chain length $\frac{1}{L^2}$ in the case of a spin-0 impurity; (b) as a function of the inverse chain length $\frac{1}{L}$ in the case of a spin-1 impurity.

## C. Adiabatic model

*Numerical technique*: As seen above, a full treatment of the lattice dynamics is tedious and restricted to small clusters. On the other hand, when $\Omega \to 0$, an adiabatic approximation of the lattice is justified and enables us to handle larger clusters both in ED or QMC calculations. The main technical issue is to find the set of distortions $\{\delta_i\}$ which minimizes the total energy, $\frac{\partial \langle \mathcal{H}_\parallel^{(\mathrm{a})} \rangle}{\partial \delta_i} = 0$, which leads to

$$J\langle \vec{S}_i \cdot \vec{S}_{i+1} \rangle + K\delta_i = 0, \qquad (6)$$

where $\langle \cdots \rangle$ is the mean value in the GS for an ED calculation or some thermal average for a QMC calculation. Eq. (6) must be solved with the constraint of zero total distortion,

$$\sum_i \delta_i = 0. \qquad (7)$$

This problem is clearly self-consistent since in the equilibrium condition (6) the distortion pattern is present in both terms: implicitly in the first one because the GS depends on it, and explicitly in the second one. Consequently this problem can be treated using the following iterative procedure.[31] First, a randomly chosen set $\{\delta_i^0\}$ satisfying (7) is taken. Applying the equilibrium condition (6), where the mean values are considered using the adiabatic Hamiltonian with the set $\{\delta_i^0\}$, gives another set $\{\delta_i'\}$ of distortions. After subtracting its mean value, a new set $\{\delta_i^1\}$ satisfying (7) is then obtained and the procedure is repeated until convergence.

This scheme can be applied using ED or QMC techniques. Note however that in this last case, although larger lattice sizes can be considered, one is restricted to

the non-frustrated $\alpha = 0$ case to avoid the minus sign problem. As expected, for a (pure) periodic chain, the static uniform dimerization pattern $\delta_i = (-1)^i \delta$ is obtained through this procedure.

*Results*: In this part, we shall study the introduction of a spin-0 or a spin-1 impurity in a chain described by the adiabatic Hamiltonian. It is here crucial to enable the magnitude of the modulation $|\delta_i|$ to vary along the chain. A QMC self-consistent method is used so that we shall restrict ourselves to the non-frustrated $\alpha = 0$ case in order to avoid sign problems. A standard world-line algorithm was implemented. Most of the calculations were performed at $T = 0.05J$ which we have shown in previous studies is low enough to reflect essentially the GS properties.[31,15,16] Besides, since we are mostly interested in GS properties we have carried on the simulations in the subspace of minimum $z$-component of the total spin. The number of slices in the Trotter direction was taken equal to $M = 120$.

Patterns of dimerization are shown in Figs. 5 and 6 for a chain with a spin-0 impurity and are similar to those observed using the dynamical approach. For even chains, the main features are identical (Fig. 5). The distortion rapidly oscillates with a two-site period with strong bonds on the edges, where the impurity lies. Its amplitude is slightly varying along the chain, the strongest distortion magnitude being observed at the edges. The magnitude of the distortion decreases when $K$ increases as seen in Fig. 5. The z-component of the spin $\langle S_i^z \rangle$ vanishes in this case because the chain is in the singlet dimer SP state.
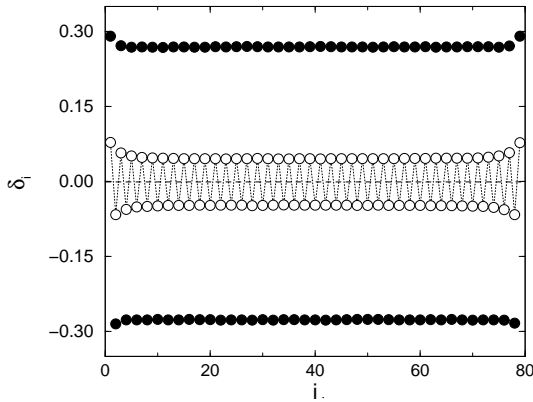


FIG. 5. Distortion patterns $\delta_i$ on a 80 site chain as a function of the position i for $\alpha = 0$, $K = J$ (•, the dotted line between the computed points is not shown for clarity) and $K = 3J$ (○) using QMC ($T = 0.05J$).

For odd chains, a single solitonic excitation is located away from the edges as shown in Fig. 6. Its presence is inferred, as previously, from a local vanishing $\delta_i$ and a maximal $\langle S_i^z \rangle$. In this case we consider the local spin susceptibility,

$$\chi_i = \frac{1}{T} \sum_j \langle S_i^z S_j^z \rangle \qquad (8)$$

instead of $\langle S_i^z \rangle$. Indeed, when using a QMC algorithm with an odd number of sites, a fictitious site has to be added and the total spin of the chain can fluctuate between $+\frac{1}{2}$ and $-\frac{1}{2}$ through spin flips with this additional spin. However, the spin susceptibility $\chi_i$ deals with a z-component of the local spin with respect to the chain *global* spin orientation[32,15]. Note that, however, this excitation is topological in nature in the sense that $\chi_i$ integrated in space on a finite region gives exactly a Curie law of a spin-$\frac{1}{2}$. The soliton width increases as the spin-phonon coupling decreases and becomes a sinusoidal distortion in the weak coupling limit.[31] In fact, the inverse soliton width, the spin gap, and the amplitude of the dimerization are three different features of the SP transition and all of them increase with the spin-phonon coupling.
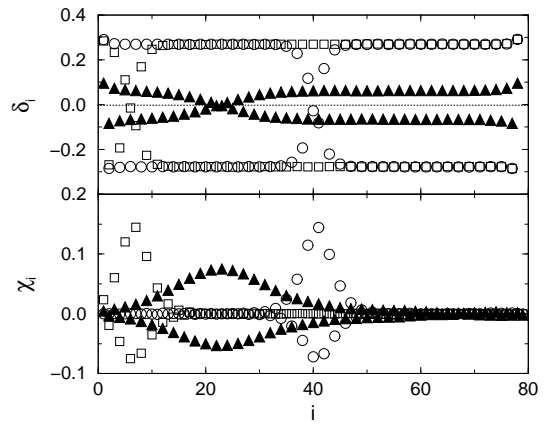


FIG. 6. Distortion $\delta_i$ (a) and magnetic susceptibility $\chi_i$ (b) patterns as a function of the position i on a 79 site chain for $\alpha = 0$, $K = J$ (○, □ correspond to two different runs) and $K = 2.5J$ (▲) using QMC ($T = 0.05J$). Lines joining computed points are not plotted for clarity.

It is interesting to notice that different QMC runs (○ and □ in Fig. 6) lead to the very same solitonic patterns centered at different sites in a large area around the middle of the chain. This is another evidence that there is no binding between non-magnetic impurities and solitons in this strictly one-dimensional model. The fact that the solitons are at least a distance away of the edges equal to half the soliton width indicates a likely short range repulsion between the soliton and the impurity.

Next, we turn to the case of a spin-1 impurity. Typical distortion and susceptibility patterns are shown in Fig. 7 for an odd length chain. In first approximation, the spin-1 impurity and its two spin-$\frac{1}{2}$ neighbors behave like a singlet,[33] *i.e.* like a spin-0 impurity as indicated by very strong bonds connected to the spin-1 impurity. This three-spin object is weakly connected to the rest of the system as indicated by particularly weak bonds ($\delta_i < 0$) between sites 1 and 2, and L-1 and L (the impurity is located at site 0).[16] Furthermore, strong bonds can even be observed close to this composite object (see arrows in

5

Fig. 7) as it is the case for a real S=0 impurity. Physically, the three-spin cluster spends most of the time in a singlet state configuration. One observes that the soliton always stays quite close to the impurity, independently of the QMC run, suggesting a small residual impurity-soliton binding, consistent with the previous dynamical calculation.
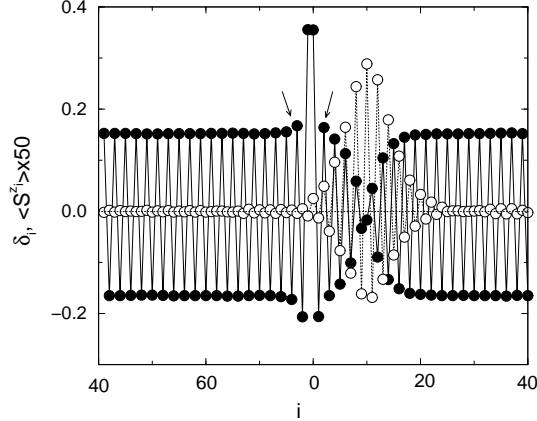


FIG. 7. Local distortion $\delta_i$ ($\bullet$) and z-component of the local spin $\langle S_i^z \rangle$ ($\circ$) as a function of the position i on a 79 site chain for $\alpha = 0$ and $K = 1.5J$ using QMC ($T = 0.05J$). A spin-1 impurity is located at site 0 at the middle of the figure and periodic boundary conditions are used. Two arrows indicate particularly strong bonds ($\delta_i > 0$) next to the spin-0 object formed by the spin-1 and its two neighbors.

## III. EXPLICITLY DIMERIZED CHAINS

The Hamiltonians considered in Sec. II are purely one-dimensional. However, in SP compounds, the phonons have a three-dimensional character. One of the simplest models proposed in the literature to take this three-dimensional behavior into account is the dimerized Heisenberg chain,

$$\mathcal{H}_{\mathrm{MF}} = J \sum_i [(1 + \delta(-1)^i)\vec{S}_i \cdot \vec{S}_{i+1} + \alpha \vec{S}_i \cdot \vec{S}_{i+1}], \quad (9)$$

where $\delta$ is an explicit dimerization. Contrary to the models considered in Sec. II, the distortion pattern is here static and uniform. It is interesting to note that this Hamiltonian (9) can in fact be inferred from the dynamical Hamiltonian (1) when only the dominant $\pi$-mode phonon is considered[27].

The dimerized Heisenberg chain has been widely studied in the literature. Its main features are the following: the elementary excitations can be interpreted as magnetic solitons and antisolitons (or spinons), namely isolated spins-$\frac{1}{2}$ separating two dimerization patterns[4,20]. As in the models considered in the previous section, for even site chains, solitons and antisolitons do not exist in this model as independent particles but appear in pairs. However, in this case, as a difference to those models,

they are confined by a linear potential proportional to $\delta(\neq 0)$ in the weak $\delta$ limit[20,34,35]. It has also been shown that the excitation spectrum is constituted of a ladder of soliton-antisoliton bound states lying below a two-magnon continuum[20,36,37]. The differences between the models studied in the previous section and the present one can be schematically visualized in the large dimerization limit as in Fig. 8. While in the fully quantum dynamical model both the distortion pattern $\{\delta_i\}$ and magnetic dimers are two-fold degenerate, in the chain with fixed dimerization only one of the distortion patterns is chosen and a magnetic state with $s\bar{s}$ pair separating two magnetic dimers configuration would leave a region with a "wrong" pattern in between the soliton and anti-soliton thus leading to a confining potential. On the other hand, this confining is absent if Hamiltonian (2) is considered since in this case the lattice would relax following the magnetic order.
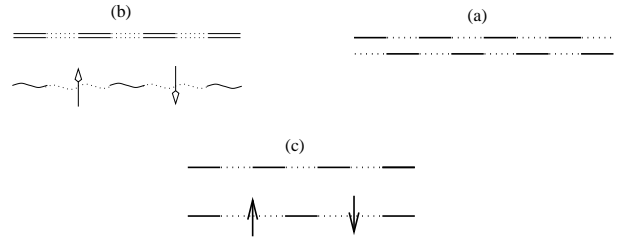


FIG. 8. (a) The two-fold degenerate GS of Hamiltonian (1). The solid (dashed) lines indicate strong (weak) bonds and dimer singlets. (b) The fixed dimerization pattern of $\mathcal{H}_{\mathrm{MF}}$ (above) and a magnetic configuration of singlet dimers with a $s\bar{s}$ pair (below). (c) A magneto-elastic state without (above) and with a $s\bar{s}$ pair (below) of Hamiltonian (2).

The case of an odd chain with open boundary conditions, i.e. with a spin-0 impurity cutting the chain, has been extensively studied in Ref. 15. It has been shown that, due to the linear confining potential, an isolated soliton binds to the spin-0 impurity next to a weak bond[15,35,36]. In this section, we generalize the approach of Ref. 15 to investigate the possibility of several bound states and to study the low energy spectrum. Following Ref. 36, we assume that the dimerization is stabilized by a strong frustration $\alpha \sim 0.5$ while the "confining force" introduced by $\delta$ remains small. The excitation spectrum with respect to the "vacuum" energy i.e. the GS energy of a periodic even chain (without any defect) interpolated to odd chains, is shown in Fig. 9. The energies could also be equivalently measured with respect to the beginning of the continuum but finite size effects affect its position making results more dependent of the lattice size. For $\alpha = 0.5$ and $\delta = 0.05$, four soliton-impurity bound states below the continuum can be clearly identified. The energy of the soliton-impurity bound state can increase up to an upper bound, above which it becomes energetically more favorable to create a soliton-antisoliton bound state. This state, which is a combination of a soliton-

impurity and soliton-antisoliton bound states, has a spin $\frac{3}{2}$ and is the lowest state of the continuum. We have checked that its energy $E_0(\frac{3}{2}) = (0.7949 \pm 10^{-4})J$, is in the thermodynamic limit the sum of the lowest impurity-soliton bound state $E_0(\frac{1}{2}) = (0.2748 \pm 10^{-4})J$ plus the lowest energy of a $s\bar{s}$ bound state, $i.e.$ the spin gap $\Delta^{01} = (0.5200 \pm 10^{-4})J$, where $\Delta^{01} = E_0(2p,1) - E_0(2p,0)$ in the notation of Eq. (4). The above energies are infinite size extrapolations obtained with ED and DMRG for $\alpha = 0.5$ and $\delta = 0.05$.
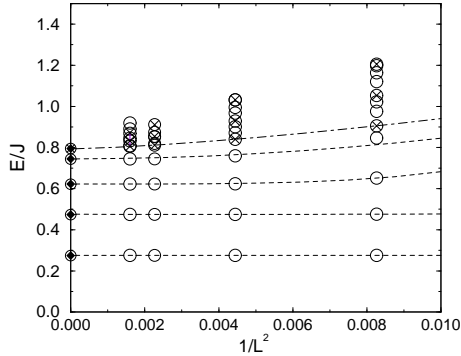


FIG. 9. Lowest lying $S^z = \frac{1}{2}$ ($\circ$) and $S^z = \frac{3}{2}$ (X) excitations for the $\alpha = 0.5$ and $\delta = 0.05$ Heisenberg chain as a function of the square inverse of the chain length L (up to L=25) obtained by ED. The energy reference is the GS of the even periodic chain interpolated to odd sizes. Dashed lines represent a $(\frac{1}{L^2}, \frac{1}{L^3})$ fit and the extrapolations to infinite sizes are indicated. DMRG extrapolations are also plotted ($\blacklozenge$). The dot-dashed line indicates the onset of the continuum.

The wave functions $\langle S_i^z \rangle$ obtained in a DMRG calculation shown in Fig. 10 clearly support this scenario. The four lowest states (a,b,c,d) show a soliton bound to the weak bond edge, and the soliton moves further away from the impurity when its energy increases. In contrast, in the lowest spin-$\frac{3}{2}$ state (Fig. 10(e)), a $s\bar{s}$ bound pair can be clearly identified in addition to the solitonic GS seen in Fig. 10(a). The number of soliton-impurity bound states below the continuum seems to increase with $\frac{1}{\delta}$, as was originally proposed for the number of $s\bar{s}$ pairs[20,36].

## IV. ELASTIC INTERCHAIN COUPLING

The three-dimensional character of phonons has been considered in Sec. III using the dimerized Heisenberg chain. However this can be achieved in a more appropriate way by adding to the pure 1D models of Sec. II an interchain coupling. Such an approach is particularly necessary for materials with large anisotropy in the elastic properties. Our motivation here is to improve the description of Sec. III in order to enable the lattice to locally relax following the magnetic order. As seen previously in the case of isolated chains, such effects are crucial in the presence of inhomogeneities introduced by

local magnetic excitations (solitons) or impurities and lead to important qualitative differences with the dimerized Heisenberg chain (9).
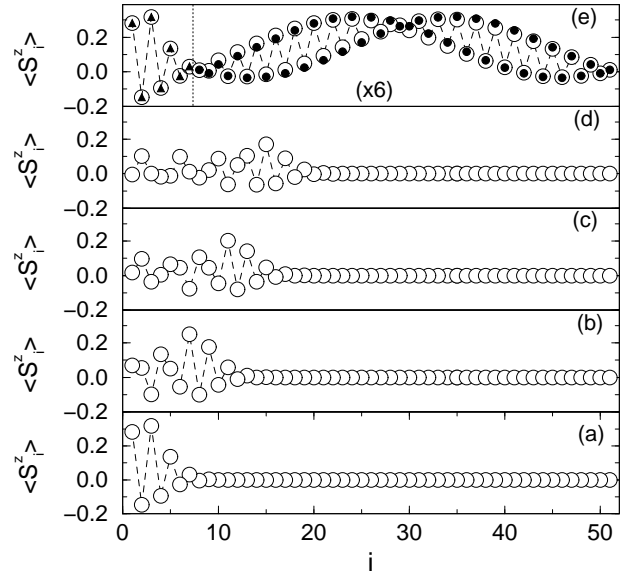


FIG. 10. $\langle S_i^z \rangle$ as the function of the site i for the four lowest spin-$\frac{1}{2}$ (a,b,c,d) and the lowest spin-$\frac{3}{2}$ state (e) for $\alpha = 0.5$, $\delta = 0.05$ on a 51-site chain using a DMRG algorithm. The bond between the first two sites is "weak". In (e), a magnification by a factor 6 has been applied to the points left to the dashed line. The 7 first sites of the lowest bound state (a) ($\blacktriangle$) and a soliton-antisoliton pair on a 44 site lattice ($\bullet$) are also shown for comparison.

In a quasi-1D SP compound, a given chain cut at its ends by spin-0 impurities ("impurity chain") is immersed in the bulk. The neighboring chains are in the SP phase, i.e. they have a uniform dimerization, and produce on this chain a $q = \pi$ potential through an elastic interchain coupling of the form[18,20],

$$\mathcal{H}_\perp = K_\perp \sum_i \delta_i \delta_i^{\text{ext}},$$

where $\delta_i$ is the distortion of the impurity chain, $\{\delta_i^{\text{ext}}\}$ are associated to the neighboring chains and $K_\perp$ is the interchain elastic coupling constant. Note that using this model, two neighboring chains can be in phase or out of phase depending on the sign of $K_\perp$. The neighboring chains can be treated in the mean-field approximation while fully retaining the dynamics of the considered chain: $\delta_i^{\text{ext}} = (-1)^{i+1}\delta_0$. Consequently, one obtains,

$$\mathcal{H}_\perp = K' \sum_i (-1)^{i+1}\delta_i,$$

where $K' = K_\perp \delta_0$.

As schematically shown in Fig. 11(a), in a strong external potential, the situation is similar to the one of Sec. III:

the soliton is bound to the spin-0 impurity at the weak bond edge. However, in a weak external potential, results of Sec. II suggest that solitons can delocalize away from the spin-0 impurity edge as depicted in Fig. 11(b) leaving strong bonds at the edges. Our aim here is to study how, when switching on an external potential and increasing it, the soliton binds to the impurity. The results shown in this part are obtained using an adiabatic treatment of the lattice and a QMC simulation of the spin degrees of freedom (similar to Sec. II C) for non-frustrated chains with spin-0 impurities. Consequently, the lattice can be seen as open chains with two unequivalent non-magnetic impurities at its edges.
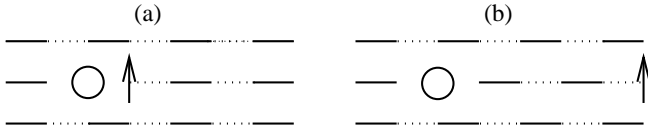


(a)          (b)

FIG. 11. Introduction of a non-magnetic impurity in a three-dimensional spin-Peierls compound. Schematic pattern pictures are drawn for the case of $K' > 0$. (a) corresponds to a strong external potential and (b) to a weak external potential. Full (dashed) lines symbolize strong (weak) bonds.

We first consider the case of an odd size chain. For vanishing $K'$, the soliton is free and strong bonds ($\delta_i > 0$) occur at the two chain ends. A non-zero $K'$ creates a linear confining potential between the soliton and the impurity where the potential tends to form a weak bond. This confining potential then equilibrates with the short range impurity repulsion. Consequently, the soliton moves to-
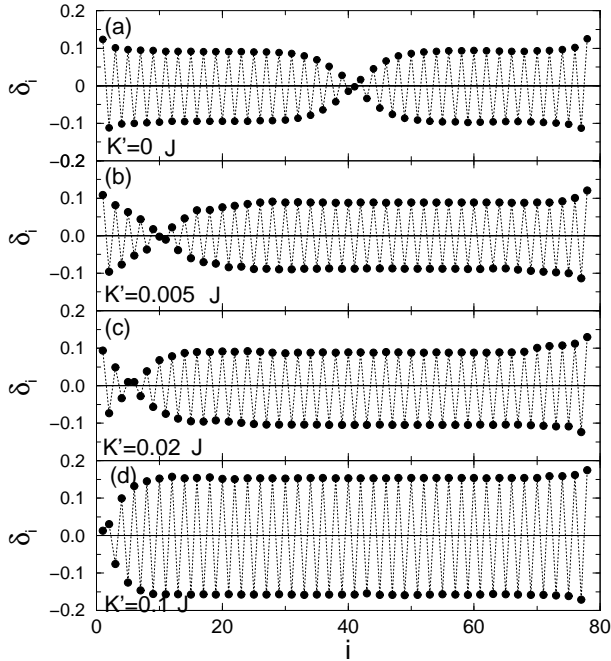
wards the impurity when the interchain coupling $K'$ increases, as can be seen in Fig. 12. Moreover, the magnitude of the dimerization increases with $K'$ as expected. Note that the distortion pattern obtained in Fig. 12(d), i.e. stronger bond on one edge and zero distortion at the other edge, is strikingly different from those of Ref. 30. These two different behaviors (obtained for $i \sim 1$ and $i \sim L$) are in fact expected on each side of any given impurity in this system.

For even size lattices, two cases have to be examined. If the free distortion pattern and the external potential are in phase (i.e. if $K'\delta_i^0\delta_i^{\text{ext}} > 0$, where $\delta_i^0 = \delta_i(K' = 0)$ ), the external potential amplifies the free distortions seen in Fig. 5 with strong bonds on the edges. However, if they are out of phase, the external potential will create two topological soliton defects. These excitations move to the chain edges and become more localized when the external potential increases, similarly to what happens for a static dimerized chain[15,36]. The patterns shown in Fig. 13 support this scenario: a spin $\pm\frac{1}{2}$ is located near each edge. Note that at low temperature, this excess of spin-$\frac{1}{2}$ at the chain's ends oscillates between positive and negative value for different QMC runs, corresponding to the $S^z \rightarrow -S^z$ symmetry. Consequently the role of the interchain elastic coupling is crucial in order to stabilize impurity-soliton bound states.
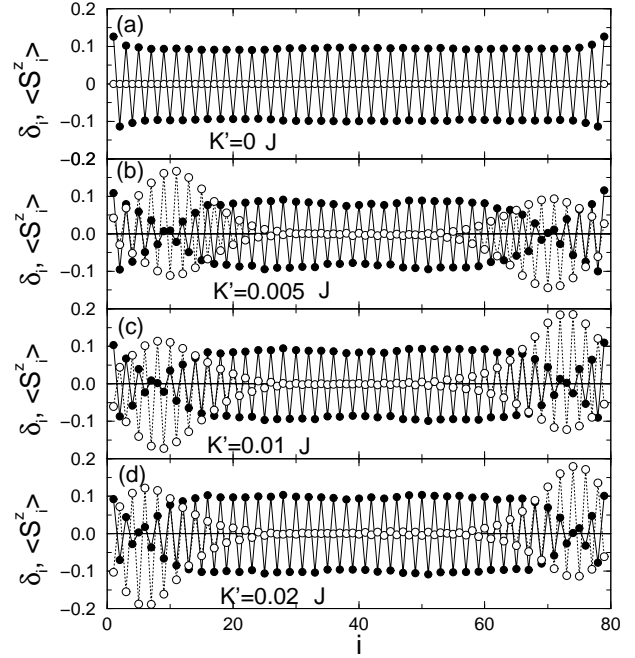


FIG. 13. Lattice distortions $\delta_i$ ($\bullet$) and z-component of spin $\langle S_i^z \rangle$ ($\circ$) as a function of the position i on a 80 site chain for $\alpha = 0$, $K = 2J$ with an interchain coupling $K'$ using QMC ($T = 0.05J$). The value of $K'$ is indicated on the graph.



FIG. 12. Lattice distortions $\delta_i$ as a function of the position i on a 79 site chain for $\alpha = 0$, $K = 2J$ with an interchain coupling $K'$ obtained by QMC simulation ($T = 0.05J$). The value of $K'$ is indicated on the graph.

The formation of the $s\bar{s}$ topological defect in the open chains with an even number of sites $L$ (as described above) is particularly subtle. In fact, because of the finiteness of the energy cost $\Delta^{01}$ (or $2e_s$ if the solitons

are far away) associated with the formation of the defect, one can, on general grounds, deduce the existence of a critical value $K'_c$ of $K'$ in such a phenomenon. A comparison between the energy cost $\propto 2e_s \simeq \Delta^{01}$ and the transversal elastic energy gain $\propto K'(L - 2\Gamma)$, where $\Gamma$ is half the soliton width, leads to $K'_c \sim \Delta^{01}/(L - 2\Gamma)$. Since $\Delta^{01}$ increases with decreasing $L$, and $\Gamma = \Gamma(K)$ is roughly independent of $L$ (see Ref. 38), then we expect that $K'_c$ decreases for increasing chain length. For $K = 2$ we have obtained $K'_c = 0.050, 0.032$ and $0.005$ for $L = 20, 40$ and $80$ respectively, thus confirming this prediction.

For real SP compounds doped with non-magnetic impurities, chains are cut at random places. By simple inspection of all possible configurations, the previous study shows unambiguously that exactly one spin-$\frac{1}{2}$ becomes bound to each impurity due to the interchain elastic coupling responsible for the three-dimensional character of the lattice dynamics provided that $K' > K'_c$. However, in chains short enough that $K'_c(L) > K'$, non-magnetic impurities at the ends do not carry magnetic moments. In other words, let us assume that one, by thought, moves closer to each other two impurities with respectively a soliton and anti-soliton bound to them. Our previous analysis shows that, below a critical separation $L_c \simeq 2\Gamma + \Delta^{01}/K'$ between the two impurities, this magnetic state becomes unstable towards a new configuration where the soliton and the antisoliton annihilate each other and leave behind a dimerization pattern in antiphase with the 3D order. Notice that such open chains are most likely to appear in the system after doping since the probability distribution of lengths is $P(L) = c(1-c)^L$, where $c$ is the impurity doping. Furthermore, the characteristic distance $L_c$ can become fairly large for small interchain elastic coupling $K'$.

Finally, in Fig. 14 we show the staggered spin-spin correlation function $C^{(s)}(|i - j|) = (1/L) \sum_{i,j} \langle \vec{S}_i \cdot \vec{S}_j \rangle (-1)^{|i-j|}$ (normalized such that $C^{(s)}(0) = 1$) for $L = 80$, $K = 2$ and $K' = 0$ and $0.02$ obtained by QMC. A clear enhancement of the AF correlations can be seen when a soliton-impurity bound state is present ($K' = 0.02$) in contrast to the case of an almost uniform pattern with strong end bonds shown in Fig. 5 ($K' = 0.0$). This result is consistent with the enhancement of AF correlations close to an impurity for weak end bonds found in Ref. 15. One expects that this increase of the AF correlations in the vicinity of impurities carrying an effective spin-1/2 magnetic moment can be observed in inelastic neutron experiments at low energy transfer and momentum transfer $q \sim \pi$.

Our results are also consistent with the experimental observation of Curie laws in the susceptibility of Zn-doped (spin-0)[10] and Ni-doped (spin-1)[11] $CuGeO_3$ materials. Note however that, in the case of Zn-doping, due to the mechanism described in Sec. IV, a significant fraction of the impurities may not carry an effective spin-1/2 leading to a reduction of the magnitude of the Curie
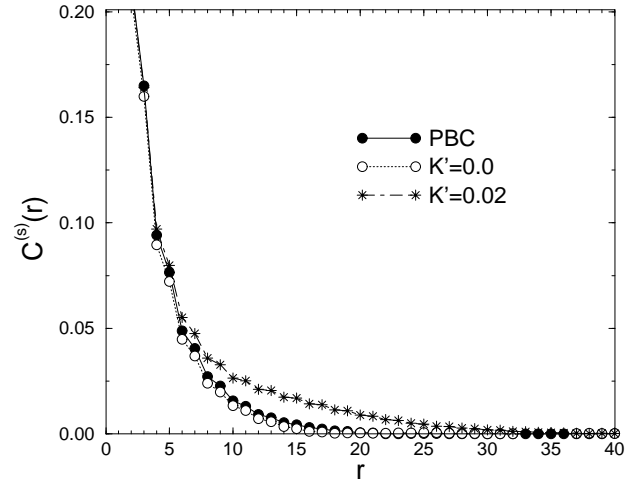


FIG. 14. Staggered spin-spin correlations in the 80 site chain with $K = 2$ obtained by QMC ($T = 0.050$). Periodic boundary conditions with $K' = 0$ and OBC with various values of the interchain coupling $K'$ as indicated on the plot have been considered.

term. In the case of Ni-doped $CuGeO_3$ (Ref. 39), an interesting cross-over at low temperature was observed between two different Curie law behaviors. We interpret this low temperature behavior with the formation of an effective singlet at the Ni-site which can bind a spin-$\frac{1}{2}$ soliton as described in Sec. II.

## V. CONCLUSION

In this work, we have studied several spin-lattice models using various numerical techniques. Local non-uniform dimerization patterns have been obtained resulting from inhomogeneities due to impurity doping. We have shown that the lattice responds strongly to the variation of the spin density even in the adiabatic case. Binding between elementary solitonic excitations and spin-S impurity (S=0 or 1) has been investigated. In strictly 1D models, no binding between solitons and non-magnetic impurities occurs. However, a small binding between spin-1 impurities and solitons has been inferred. The role of the three-dimensionality of the lattice was also investigated by comparing a model with a fixed mean field-like dimerization to a model with an explicit coupling to an adiabatic lattice which can locally relax to follow the magnetic order. In the latter case, the interchain elastic coupling was shown to be responsible for the binding of solitons to spin-0 impurities. However, in contrast to the dimerized Heisenberg model, we predict in this model the existence of $S = 0$ impurities carrying no spin-1/2 solitonic excitation. These impurity sites must appear in pairs separated by sufficiently small chain segments with an even number of sites and a dimerization pattern in antiphase with respect to the 3D dimerization order.

## VI. ACKNOWLEDGEMENTS

[1] M. Hase, I. Terasaki and K. Uchinokura, Phys. Rev. Lett. **70** 3651 (1993).

[2] M. Isobe and Y. Ueda, J. Phys. Soc. Jpn. **65**, 1178 (1996).

[3] For a review on $CuGeO_3$, see E.g. J.P. Boucher and L.P. Regnault, J. Phys. I (Paris) **6**, 1939 (1996).

[4] B. Shastry and B. Sutherland, Phys. Rev. Lett **47**, 964 (1981).

[5] J. Riera and A. Dobry, Phys. Rev. B **51**, 16098 (1995).

[6] G. Castilla, S. Chakravarty and V.J. Emery, Phys. Rev. Lett. **75**, 1823 (1995).

[7] M. Hase, I. Terasaki, Y. Sasago, K. Uchinokura, and H. Obara, Phys. Rev. Lett. **71**, 4059 (1993).

[8] J.G. Lussier, S.M. Coad, D.F. McMorrow, and D. McK. Paul, J. Phys. Cond. Matt. **7**, L325 (1995).

[9] S.B. Oseroff, S-W. Cheong, B. Aktas, M. F. Hundley, Z. Fisk, and L. W. Rupp, Jr., Phys. Rev. Lett. **74**, 1450 (1995).

[10] T. Masuda, A. Fujioka, Y. Uchiyama, I. Tsukada, and K. Uchinokura, Phys. Rev. Lett. **80**, 4566 (1998); K. Manabe, H. Ishimoto, N. Koide, Y. Sasago, and K. Uchinokura, preprint cond-mat/9805072.

[11] N. Koide, Y. Uchiyama, T. Hyashi, T. Masuda, Y. Sasago, K. Uchinokura, K. Manabe, and H. Ishimoto, preprint cond-mat/9805095.

[12] L.-P. Regnault, J.-P. Renard, G. Dhalenne, and A. Revcolevschi, Europhys. Lett. **32**, 579 (1995).

[13] L.-P. Regnault, M. Aïn, B. Hennion, G. Dhalenne, and A. Revcolevschi, Phys. Rev. B **53**, 5579 (1996).

[14] G.B. Martins, E. Dagotto and J. Riera, Phys. Rev. B **54**, 16032 (1996).

[15] M. Laukamp, G. B. Martins, C. Gazza, A. L. Malvezzi, E. Dagotto, P. M. Hansen, A. C. López and J. Riera, Phys. Rev. B **57**, 10755 (1998).

[16] P.M. Hansen, J.A. Riera, A. Delia and E. Dagotto, Phys. Rev. B **58**, in press (1998).

[17] D. Poilblanc, in *Numerical Methods for Strongly Correlated Systems*, edited by D. J. Scalapino (Frontiers in Physics, 1997).

[18] D. Khomskii, W. Geertsma, and M. Mostovoy, Czech. J. Phys., **46**, Suppl. S6, 3239 (1996).

[19] D. Augier, D. Poilblanc, E. Sørensen and I. Affleck, preprint cond-mat/9802053, to be published in Phys. Rev. B (1998).

[20] I. Affleck, Proceedings of the NATO ASI: Dynamical properties of Unconventional Magnetic Systems, April, 1997, cond-mat/9705127.

[21] P. Hansen, D. Augier, J. Riera, and D. Poilblanc, preprint cond-mat/9805325.

[22] F. D. M. Haldane, Phys. Rev. B **25**, 4925 (1982).

[23] K. Okamoto and K. Nomura, Phys. Lett. A **169**, 433 (1992); R. Chitra, S. Pati, Krishnamurthy, D. Sen, and S. Ramasesha, Phys. Rev. B **52**, 6581 (1995).

[24] S. R. White and I. Affleck, Phys. Rev. B **54**, 9862 (1996).

[25] S. Eggert, Phys. Rev. B **54**, 9612 (1996).

[26] A.W. Sandvik, R.R.P. Singh, and D.K. Campbell, cond-mat/9706046.

[27] D. Augier and D. Poilblanc, Eur. Phys. J. B **1**, 19 (1998).

[28] G. Wellein, H. Fehske, and A.P. Kampf, preprint cond-mat/9804085.

[29] R. Fehrenbacher, Phys. Rev. Lett. **77**, 2288 (1996); R. Fehrenbacher, Phys. Rev. B **49**, 12 230 (1996).

[30] H. Fukuyama, T. Tanimoto, and M. Saito, J. Phys. Soc. Jpn. **65**, 1182 (1996).

[31] A.E. Feiguin, J.A. Riera, A. Dobry, and H.A. Ceccatto, Phys. Rev. B **56**, 14 607 (1997); see also F. Schönfeld, G. Bouzerar, G.S. Uhrig and E. Müller-Hartmann, preprint cond-mat/9803084.

[32] S. Eggert and I. Affleck, Phys. Rev. Lett. **75**, 934 (1995).

[33] S. Eggert and I. Affleck, Phys. Rev. B **46**, 10866 (1992).

[34] G.S. Uhrig and H.J. Schulz, Phys. Rev. B **54**, R9624 (1996); A. Fledderjohann and C. Gros, Europhys. Lett. **37**, 189 (1997); D. Augier, D. Poilblanc, S. Haas, A. Delia, E. Dagotto, Phys. Rev. B **56**, R5732 (1997).

[35] G. S. Uhrig, F. Schönfeld, M. Laukamp and E. Dagotto, preprint 9805245.

[36] E. Sørensen, I. Affleck, D. Augier and D. Poilblanc, preprint cond-mat/9805386 (1998).

[37] G. Bouzerar, A.P. Kampf, and G.I. Japaridze, preprint condmat/9801046.

[38] The soliton width depends also on the elastic interchain coupling as reported in A. Dobry and J. Riera, Phys. Rev. B **56**, 2912 (1997).

[39] B. Grenier, J.-P. Renard, P. Veillet, C. Paulsen, G. Dhalenne, and A. Revcolevschi, submitted to Phys. Rev. Lett. (1998).